PHYSICAL REVIEW B VOLUME 26, NUMBER 2 15 JULY 1982

Hyperfine fields and electronic structure of hydrogen impurities in transition metals

B. Lindgren* and D. E. Ellis
Department of Physics and Astronomy and Materials Research Center, Northwestern University, Evanston, Illinois 60201
(Received 22 February 1982)

The hyperfine fields and charge and spin densities around hydrogen impurity sites in iron, cobalt, and nickel are calculated using the local-density formalism in an embedded cluster model. The sensitivity of the self-consistent spin density to embedding constraints and the cluster boundary conditions is explored. A continuum-state boundary condition is developed which serves to broaden the discrete cluster levels in a physically satisfactory manner. The hyperfine field is seen to result from a delicate balance between negatively exchange-polarized "bound-paired" states and positive "unpaired-band" contributions. The theory shows a reduction in moment for atoms around the impurity site as observed; the calculated moments and fields are in fairly good agreement with experiment, using up to 38 atom clusters. The pressure dependence of the *muon* hyperfine field is presented.

I. INTRODUCTION

The electronic structure of impurities in metals is a fascinating problem. In particular, the electronic structure of light impurities, such as hydrogen, has become a topic of great current interest because of its important technical applications. A number of interesting consequences for many metallic characteristics, such as magnetic, superconducting, and mechanical properties as well as many technical applications, has prompted the extensive recent interest in them. In particular, the muon spin rotation technique has emerged as a powerful probe to study spin densities, crystallographic position, diffusion properties, etc.[1] Although a proton (or the lighter muon) with no core electronic structure is the simplest kind of impurity that can be implanted into a solid, the electronic structure of the proton in metals is a surprisingly complicated subject and a number of theoretical models have been developed.[2] In the jellium model, the periodic lattice structure is neglected and the positive charges on the host ions are smeared out uniformly to form a homogeneous density background. The screening of the impurity is then treated in standard linear[3] or nonlinear screening theories.[4–6] In metals with small ion cores and no d- or f-like electrons, such continuum-based approaches are justifiable and discrete lattice effects can be accounted for perturbatively.[7] Transition metals with d bands crossing the Fermi level pose a more difficult challenge. Solving the Dyson equation for the isolated impurity problem using Korringa-Kohn-Rostoker Green's-function techniques[8] has shown considerable promise for defect studies in general. The band-structure methods with large unit cells, the "supercell" methods, certainly provide a powerful though relatively expensive approach to dilute impurities in metals.

Related to the band methods, but requiring much less computational effort, is the "molecular" approach utilizing a finite cluster of host atoms surrounding the impurity. A main problem in using cluster models to interpret properties of solids is the choice and implementation of physically reasonable embedding conditions for the cluster.[9] This implies construction of a model Hamiltonian containing cluster-environment interaction (hopefully self-consistent) and imposing suitable boundary conditions on the cluster wave functions. A spherical Wigner-Seitz boundary condition can be extended to the multiple-scattering $X\alpha$ scheme[10] where the approximation of a spherical potential within atomic spherical regions is retained and partial wave expansions are thus possible to exploit.[11] Other methods, such as the linear combination of atomic orbitals (LCAO) Hartree-Fock and discrete variational (DV) $X\alpha$ schemes, emphasize instead the multicenter mixing and on-site hybridization of atomic basis functions in the potential field of solids. In the variational method, a boundary condition is not readily usable because of the built-in decay of LCAO-type basis functions. In Sec. II we instead describe an alternative method where an

asymptotic condition is imposed on the cluster wave-function solutions.

As for hydrogen in transition metals, only a few first-principles spin-polarized calculations have been carried out. Keller[12] briefly reports calculations using an embedded cluster and the multiple-scattering technique. Kanamori *et al.*[13] used the Korringa-Kohn-Rostoker Green's-function technique, while the only spin-polarized band calculation carried out to self-consistency is the thin-film supercell study of Ni_5H by Jepsen *et al.*[14] These calculations show that a considerable part of the hyperfine field (i.e., contact spin density) arises from electronic states close to the Fermi energy. Thus we have chosen these systems to test the theoretical model described in Sec. II; in Sec. III we calculate the electronic structure of isolated hydrogen impurities in iron, cobalt, and nickel by the LCAO-DV scheme. The hyperfine field, as experienced by positive muons, is calculated and compared to experimental results and theoretical calculations by other first-principles methods. This hyperfine field is found to be determined by a delicate balance between negatively exchange polarized "bound-paired" states and a positive contribution from "unpaired-band" states at the Fermi level. In any cluster method giving discrete energy levels as a result, calculation of the latter positive term requires a prescription for broadening of the discrete levels. We also present, for the first time, a calculation of the pressure dependence of the muon hyperfine field.

II. THEORETICAL MODEL AND COMPUTATIONAL PROCEDURE

A. The Hartree-Fock-Slater model

The local-density formalism is used in carrying out molecular-orbital (MO) calculations on a finite cluster of atoms. The MO eigenstates are expanded in terms of symmetry orbitals:

$$\psi_n(\vec{r})=\sum\chi_j(\vec{r})C_{nj} \ . \tag{1}$$

The symmetry orbitals χ_j are chosen here as linear combinations of atomic orbitals located on the different atoms, corresponding to the cluster point-group symmetry.

The variational coefficients C_{nj} are obtained by solving the secular equation of the discrete variational method. This method has been described in detail elsewhere,[15,16] but for completeness we repeat the main steps. The single-particle equation

$$(h-\epsilon_n)\psi_n(\vec{r})=0 \tag{2}$$

is approximately solved by minimizing certain error moments on a diophantine sampling grid in $\vec{r}$,

$$\langle\chi_i\,|\,h-\epsilon\,|\,\psi\rangle=0 \ . \tag{3}$$

The effective Hamiltonian for state of spin σ is given (in Hartree units) by

$$h_\sigma=-\tfrac{1}{2}\nabla^2+V_{\rm Coul}+V_{{\rm ex},\sigma} \ , \tag{4}$$

where the first two terms are the kinetic energy and Coulomb potential. The von Barth–Hedin[17] potential was adopted for the spin-dependent local-density exchange,

$$V_{{\rm ex},\sigma}=[\mu_x^p(\rho)+\nu_c(r_s)]\left[\frac{2\rho_\sigma}{\rho}\right]^{1/3}+[\mu_c^p(r_s)-\nu_c(r_s)] \ , \tag{5}$$

where ρ_σ is the spin component of the total electron density $\rho=\rho_\uparrow+\rho_\downarrow$ and

$$\mu_x^p(\rho)=-\left[\frac{3\rho}{\pi}\right]^{1/3} \ ,$$

$$r_s=\left[\frac{3}{4\pi\rho}\right]^{1/3} \ ,$$

$$\mu_c^p(r_s)=-C_p\ln(1+r_p/r_s) \ ,$$

$$\nu_c(r_s)=-\frac{4(2)^{-1/3}}{3(1-2^{-1/3})}\times[C_F F(r_s/r_F)-C_p F(r_s/r_p)] \ ,$$

$$F(z)=(1+z^3)\ln(1+1/z)+z/2-z^2-\tfrac{1}{3} \ .$$

The parameters $C_p=0.0225$ a.u., $C_F=C_p/2$, $r_p=21$, and $r_F=2^{4/3}r_p$ were those suggested by Moruzzi *et al.*[18]

The matrix secular equation $(H-ES)C=0$ where H and S are the Hamiltonian and overlapping matrices, respectively, is solved by standard procedures. Since the discrete energy eigenvalues obtained for the molecular cluster is a sampled representative for energy bands in a metal, we broadened each energy level with a procedure described in detail below. Fermi-Dirac statistics were invoked on these broadened states to determine the Fermi energy and occupation numbers $f_n(\epsilon)$ for each MO. The cluster charge density was then constructed by summing over all MO's:

$$\rho_{\text{cluster}}=\sum f_n \mid \psi_n(\vec{r}) \mid^2 . \tag{6}$$

In order to calculate the potential by one-dimensional integrations, this charge density was cast in a multicenter-overlapping multipolar form,[19]

$$\rho_{\text{model}}(\vec{r})=\sum_{njlm} d_{jlm}(n)\rho_j(r_n)Y_{lm}(\hat{r}_n) \tag{7}$$

with $\vec{r}_n=\vec{r}-R_n$.

The radial density basis set $\{\rho_j\}$ was constructed from spherical atomic densities, calculated from the wave-function variational basis, and from five parabolic radial functions for each $l \leq 1$ in the fully symmetric representation of the molecular point group. The coefficients $\{d\}$ were determined by least-squares fitting to the eigenvector density of Eq. (6). Higher l terms were found not to alter the results significantly.

B. Asymptotic boundary condition

The sharp details of the energy density of states (DOS), due to the finite number of valence levels in an isolated cluster, are not relevant in an approximate description of a bulk crystal. A frequently used procedure to obtain a smoothed spectral density is to smear each energy level by a Lorenzian with a constant width:

$$D(E)=\sum_n \frac{\lambda/\pi}{(E-\epsilon_n)^2+\lambda^2} . \tag{8}$$

The main drawback of this method is that all levels are smeared equally, independent of their character as localized or diffuse states. Energy-dependent (or $\vec{k}$-wave-vector-dependent) boundary conditions can overcome this limitation[9,11] but are not easy to impose on the LCAO-type of basis used here.

We instead require that the solutions to the Hamiltonian [Eq. (4)] have a certain asymptotic form ϕ_k at the energy E_k. By asymptotic we here mean $r \to \infty$, where the tails of the atomic orbitals in (1) have vanished. The requirement can be fulfilled if the function ϕ_k is included in a new expansion of the wave function:

$$\psi(\epsilon_k,\vec{r})=a_k\phi_k+\sum_{j=1}^{N} c_j\Phi_j . \tag{9}$$

As earlier, we solve the single-particle equation (2) by minimizing error moments with respect to the variational coefficients c_j, but not a_k. We have

$$\langle \Phi_i \mid h-\epsilon_k \mid \psi \rangle=0, \quad i=1,2,\ldots,N . \tag{10}$$

This leads to an inhomogeneous equation system in $\{c\}$:

$$\sum_j \langle \Phi_i \mid h-\epsilon_k \mid \Phi_j \rangle c_j=-\langle \Phi_i \mid h-\epsilon_k \mid \phi_k \rangle a_k , \quad i=1,2,\ldots,N . \tag{11}$$

A particularly simple form is obtained by choosing Φ_i as the orthonormalized eigenfunctions to the homogeneous problem of the isolated cluster, i.e., Eq. (3), and with ϕ_k being an eigenfunction to some model Hamiltonian

$$[-\tfrac{1}{2}\nabla^2+V_0(r)]\phi_k=\epsilon_k\phi_k , \tag{12}$$

Eq. (11) reduces to

$$(\epsilon_i-\epsilon_k)c_i=-\langle \Phi_i \mid u \mid \phi_k \rangle a_k . \tag{13}$$

Here u is the difference between the cluster potential [see Eq. (4)] and V_0. In the Appendix we give an alternative derivation of these equations based on the Green's-function formalism.

Volume normalizing and separating into orthogonal terms, the new single-particle wave function becomes

$$\tilde{\psi}_k=\frac{a_k}{\langle \psi_k \mid \psi_k \rangle^{1/2}}\left[\sum_i \left[\frac{\langle \Phi_i \mid u \mid \phi_k \rangle}{\epsilon_k-\epsilon_i}+\langle \Phi_i \mid \phi_k \rangle\right]\Phi_i + \left[[\phi_k-\sum_j \Phi_j\langle \Phi_j \mid \phi_k \rangle]\right]\right] . \tag{14}$$

If $\{\Phi\}$ is a complete function set, the last term is zero. This is never true with a localized finite-numbered basis set. We may consider that $\tilde{\psi}$ is composed of two orthogonal parts, the first of which is associated with cluster-localized states. We used this part to determine properties of the embedded cluster. The probability that we will find the cluster state Φ_i at energy ϵ is thus proportional to

$$\mid d_i(\epsilon) \mid^2 \propto \frac{\left| \frac{\langle \Phi_i \mid u \mid \phi \rangle}{\epsilon-\epsilon_i}+\langle \Phi_i \mid \phi \rangle \right|^2}{\sum_j \left[\left| \frac{\Phi_j \mid u \mid \phi \rangle}{\epsilon-\epsilon_j} \right|^2 +2\langle \Phi_j \mid \phi \rangle \frac{\langle \Phi_j \mid u \mid \phi \rangle}{\epsilon-\epsilon_j} \right]+\langle \phi \mid \phi \rangle} . \tag{15}$$

By an energy normalization we may set $\int |d_i|^2 d\epsilon = 1$; thus one electron is distributed over each cluster spin orbital. The actual population is determined by integrating $|d_i|^2$ up to the Fermi energy.

Therefore, we can interpret d_i^2 as the line profile or density of states arising from cluster level i. The total density of states analogous to Eq. (8) can be written as

$$D(E)=\sum_n |d_n(E)|^2 . \tag{16}$$

Notice that Eq. (15) is also valid for $\epsilon=\epsilon_i$ and that if $\langle \Phi_i | u | \phi \rangle$ is slowly varying with energy, $|d_i|^2$ approaches a Lorenzian function with width

$$|\langle \Phi_i | u | \phi \rangle / \langle \phi | \phi \rangle^{1/2}|$$

as $\epsilon \rightarrow \epsilon_i$. Also notice that the expression is not dependent on the actual amplitude of asymptotic function ϕ. However, there is a dependence on the choice of integration volume through the term $\langle \phi | \phi \rangle$ in particular, if ϕ is not a square integrable function.

In the derivation of Eq. (15) no restriction on V_0 and the type of asymptotic function ϕ_k [see Eq. (12)] has been made. As a simple example we chose the plane wave $e^{i\vec{k}\cdot\vec{r}}$ in order to simulate propagating states in a periodic lattice. The minimum integration volume not truncating the atomic orbitals was chosen and a constant potential V_0 was set at the bottom of the valence energy levels. The exact level profile [Eq. (15)] and thus the structure of the DOS were slightly dependent on these choices and on the integration accuracy. However, since the integrated population was fed back to the potential on subsequent iterations, the converged self-consistent charge and spin densities were found to be insensitive to those parameters.

C. Basis sets

The atomic orbitals used in the molecular-orbital expansion were obtained by solving the self-consistent free-atom problem. Several numerical free-atom basis sets were considered in these calculations. A reduced overlap between orbitals on different atomic sites produces an improved variational basis but the limited spatial extent of valence orbitals should not be so great as to significantly affect diffuse conduction-electron states. Also the atomic core orbitals should not be distorted appreciably. Spherical wells of varying depth and radial extent were added to the atomic potentials so that different basis sets could be constructed. For the transition metals Fe, Co, and Ni, a well of depth 0.2 a.u. with sloping walls beginning at 5 a.u. best satisfied the criteria listed above. This basis set consisted of $3d$, $4s$, and $4p$ orbitals with the core frozen. For the hydrogen impurity (or muon), $1s$, $2s$, and $2p$ orbitals were calculated with a well of depth 5 a.u. with sloping walls beginning at 4 a.u. Since we were mainly interested in the hyperfine fields, both $1s$ and $2s$ orbitals were included in the basis set in order to ensure that the variational freedom was enough to describe the different radial behavior of orbitals of different spin.

III. HYDROGEN IN IRON, COBALT, AND NICKEL

In hcp Co the muon site has been determined to be the octahedral interstitial site through consideration of the magnetic dipolar field distribution as the easy axis of magnetization changes in the temperature range 500 to 600 K.[1] Although no unambiguous site determination has been done for the fcc phase, it is generally assumed that the muon also occupies this site in fcc Co and Ni. Neutron diffraction[20] also verifies this site for hydrogen in Ni. Therefore, only the octahedral sites were considered in the calculations with fcc Ni and fcc Co. No magnetic dipolar field is present here due to the cubic symmetry. At the noncubic interstitial tetrahedral or octahedral sites in bcc Fe, the dipolar fields seen by muons are averaged to zero because of rapid diffusion between crystallographically equivalent but magnetically inequivalent sites.[1] Both the tetrahedral and octahedral sites were considered in our calculations as well as the substitutional site, inspired by recent experimental data on vacancy trapped muons.[21] The hcp phase of Co was not included in the present work because of a more complicated analysis required with a nonvanishing dipolar field.

Since the cluster boundary condition least affects the electron density at the center of a cluster, the muon was placed at the origin surrounded with 2–3 shells of host atoms. The cluster geometries which were used are shown in Fig. 1. For comparison with host properties, calculations were also made without the muon present using the same cluster geometries.

Total densities of states (TDOS), $D(E)$, with the hydrogen present, are displayed in the top portions of Figs. 2–4. The visible difference in details of

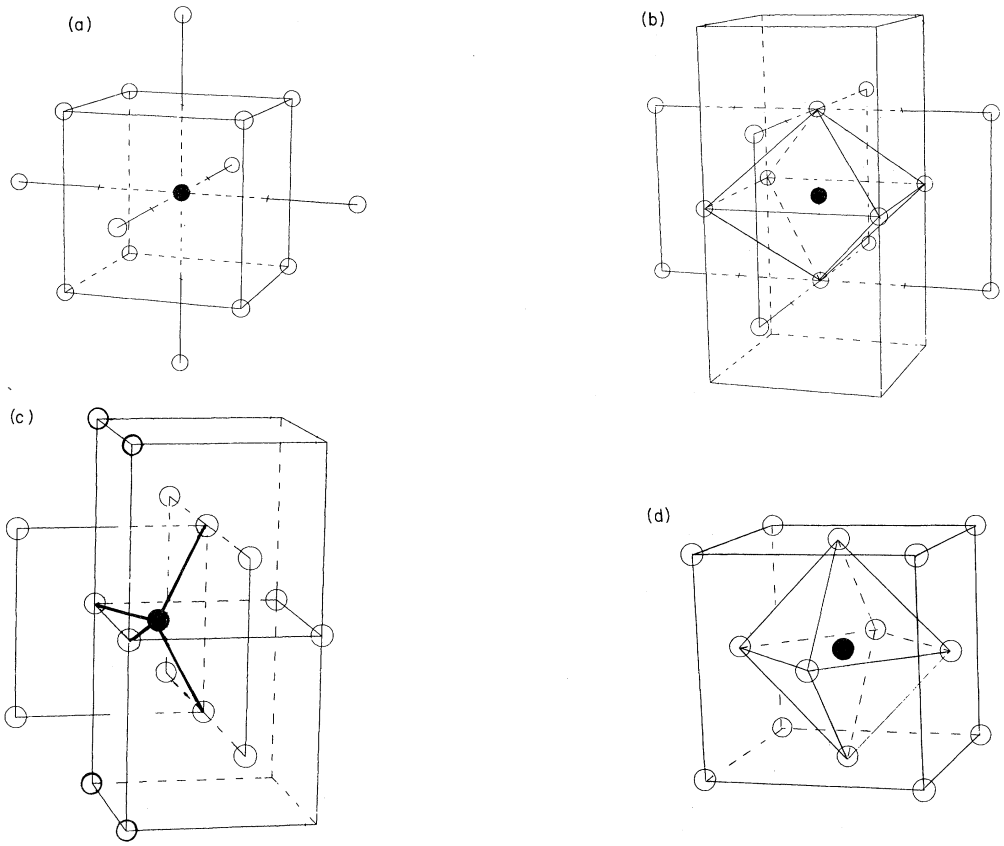

FIG. 1. Cluster geometries used for (a) substitutional site in bcc Fe, (b) octahedral interstitial site in bcc Fe, (c) tetrahedral interstitial site in bcc Fe, and (d) octahedral interstitial site in fcc Co and Ni. Filled symbol denotes hydrogen positions and unfilled symbols show host-atom positions.

the TDOS between the HFe_{14} cluster with D_{4h} point symmetry[22] and the HFe_{16} cluster with the lower D_{2d} symmetry has no significance. It merely reflects the difference in integration accuracy and in plane-wave projection onto different symmetry representations. Integrated DOS are nearly invariant as mentioned in Sec. II. Without the muon, the Fe_{14},Fe_{16} TDOS are essentially the same except for the appearance of a low-lying peak 9 eV below the Fermi energy (E_F) and outside the TDOS plot range in Figs. 2—4. This level is mainly of H 1s character and has also been observed by Jepsen *et al.*[14]

The average magnetic moment per Fe atom in the pure Fe_{14} and Fe_{16} clusters was $2.8\mu_B$. Since none of the Fe atoms in these cluster geometries is surrounded by all its neighbors, one may expect a moment between the experimental bulk value of $2.2\mu_B$ and the free-atomic value of $3\mu_B$, as obtained by Hund's rule and assuming the $3d^7 4s$ configuration in the metal. A test calculation with a Fe atom at the origin, surrounded by its eight first neighbors and six second neighbors, also gave an average moment of $2.8\mu_B$, while the moment on the center atom was $2.1\mu_B$. The average magnetic moments in the Co_{14} and Ni_{38} cluster were $1.9\mu_B$ and $0.6\mu_B$, respectively, comparing well with the experimental values of $1.7\mu_B$ and $0.6\mu_B$. Adding the H atom to the clusters caused the moment in the first-neighbor host atoms to decrease by between 0.1 and $0.2\mu_B$ in all cases. First-neighbor moments were taken as the 3d moment from a Mulliken spin-density analysis[23] of the eigenvectors.

A. Hyperfine fields

The energy dependence of the local density of states (LDOS) is defined as

$$\rho_\sigma(\vec{R},E)=\sum_n |d_{n\sigma}(E)|^2 |\Phi_{n\sigma}(\vec{R})|^2 . \quad (17)$$

Their difference defines the local spin density,

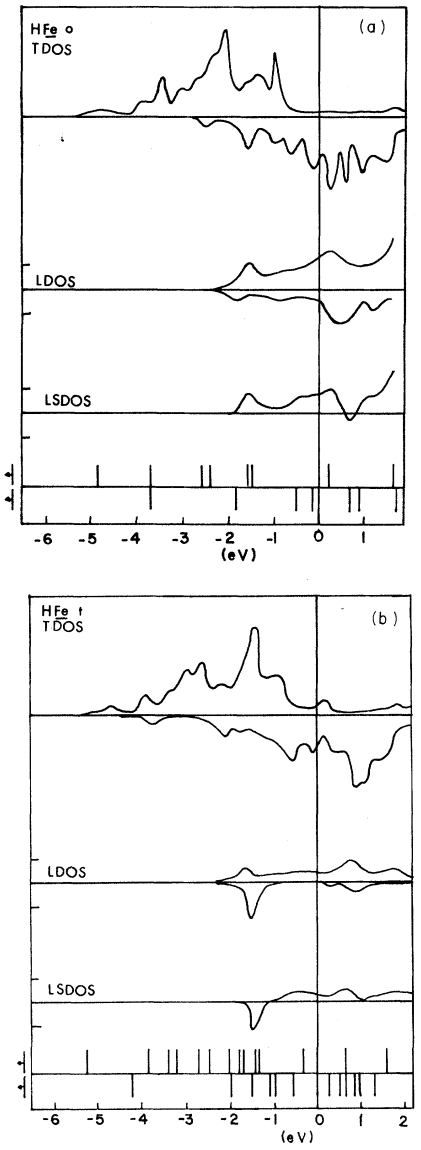

FIG. 2. Total density of states (TDOS) for spin ↑, ↓, local density of states (LDOS), and local spin density (LSDOS) for (a) octahedral position H and (b) tetrahedral position H in Fe cluster. Energy levels with density at the H site are indicated in the lower panel.

$\delta\rho(\vec{R},E)=\rho_\uparrow-\rho_\downarrow$. Here ↑ denotes majority spin, parallel to the host magnetic moment. The energy-integrated spin density at the muon site $\vec{R}$ determines the hyperfine fields,

$$B_{\rm hf}=52.42\int^{E_F}\delta\rho(\vec{R},E)dE \qquad (18)$$

in units of tesla (T).

We distinguish between two contributions:

(i) A negative contribution B_1 arises from paired states of energies more than ~ 2 eV below E_F, i.e., states which are equally populated for both spins.

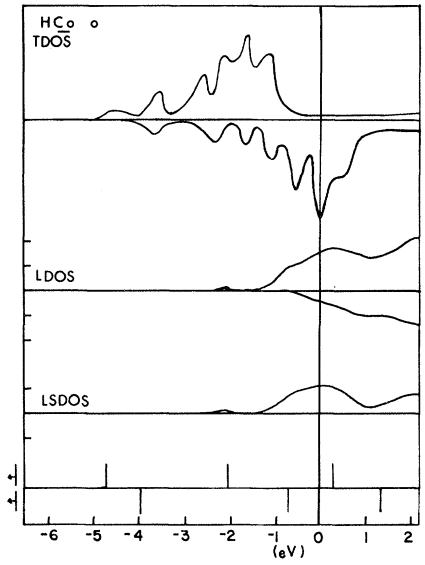

FIG. 3. Total density of states (TDOS) for spin ↑, ↓, local density of states (LDOS), and local spin density (LSDOS) for octahedral position H in Co cluster. Energy levels with density at the H site are indicated in the lower panel.

This negative density at the muon site is due to the exchange interaction with a more or less localized host d moment giving a different radial shape for the spin-up and -down wave functions.

(ii) The negative field B_1 is balanced by a positive contribution B_2 arising from the higher population of spin-up states. The energy dependence of

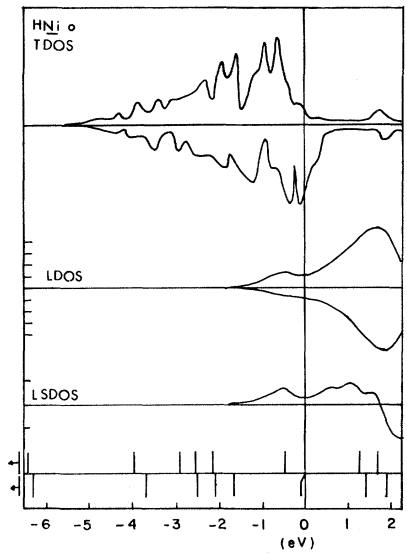

FIG. 4. Total density of states (TDOS) for spin ↑, ↓, local density of states (LDOS), and local spin density (LSDOS) for octahedral position H in Ni cluster. Energy levels with density at the H site are indicated in the lower panel.

the local density and spin density from the unpaired states are shown in Figs. 2–4 where the energy levels belonging to the fully symmetric representation of the point group are also indicated. These are the only states having a density at the origin. Calculated hyperfine fields for the different clusters are given in Table I together with the magnetization in tesla at the interstitial site without H impurity.

The general agreement between calculated B_{hf} and experimental values is quite good considering that these results are for a nonrelaxed lattice and neglect the zero-point motion of the light muon. The paired contribution B_1 in Ni agrees well with the spin density from bound states, -0.24 T, obtained by Kanamori *et al.*[13] and indicates that our basis set with the compressed 1*s* and 2*s* orbitals on H is able to describe the different radial behavior for spin-up and spin-down wave functions. Since B_2 can be expected to depend on the number of states close to E_F, we increased the number of Ni atoms from 14 to 38. The change in B_{hf} was minimal, $B_{hf}=-0.15$ T for the smaller cluster and -0.13 T for the larger one. All results given in the tables and figures are for the larger cluster. As we will show later, lattice relaxation around the muon or hydrogen atom cannot explain the difference between the theoretical and experimental values in nickel. Although the relative difference is $\sim 50\%$, the absolute deviation is not bigger than in the Fe and Co host, where the higher magnetic moment gives much higher spin densities. The basic limitations of our model for broadening the discrete cluster energy levels seem to be reached. Hence the better agreement between the calculated B_{hf} at the octahedral position in Fe should not be taken as a support for this position in preference to the tetrahedral site. The difference between the hyperfine fields at the two positions is, in fact, much smaller than the difference in dipolar fields so that diffusion between octahedral and tetrahedral positions[25] cannot be excluded by these calculations.

A calculation with the muon at a substitutional Fe vacancy gave a hyperfine field of -0.84 T with $B_1=-2.41$ and $B_2=+1.57$ T. At this site the positive peak in B_2 at E_F was much higher and sharper than for the interstitial sites. The negative net field disagrees with the preliminary calculations by Kanamori *et al.*,[13] but is in good agreement with the measured field -0.95 T for a muon trapped at iron monovacancies.[21]

B. Volume dependence and lattice distortion

Since a change in the spin density with a change in the neighbor distance may be calculated more accurately than the absolute hyperfine fields, we carried out several calculations with different lattice constants. The results are summarized in Table II. Three major effects were found with a uniformly compressed lattice:

(i) The paired contribution B_1 decreased in magnitude (less negative) and the relative volume dependence almost followed that of the nearest-neighbor host moment.

(ii) Energy levels close to E_F were shifted upwards in energy, relative to E_F, depopulating those states (antibonding states predominate).

TABLE I. Muon hyperfine fields. First column gives the host and site used in the calculations *o* = octahedral, *t* = tetrahedral interstitial sites. Columns 2 and 3 give the paired (B_1) and unpaired (B_2) contributions to the hyperfine field (B_{hf}) (column 4). Experimental value is given in column 5. The last two columns give the calculated and experimental interstitial magnetizations in tesla, without the muon impurity present.

	Muon hyperfine field				Interstitial magnetization (T)	
Host and site	B_1	B_2	$B_{hf}=B_1+B_2$	Expt. (Ref. 1)	Calculated[b]	Expt. (Ref. 24)
bcc Fe *o*	−1.73	+0.45	−1.28	−1.11	−0.01	+0.10
bcc Fe *t*	−1.69	+0.25	−1.44		−0.06	−0.16
fcc Co *o*	−1.03	+0.57	−0.46	−0.58[a]	−0.06	? −0.16 hcp
fcc Ni *o*	−0.22	+0.09	−0.13	−0.07	−0.02	−0.07

[a] Extrapolated to 0 K from 700 K. In hcp Co the experimental B_{hf} is -0.61 T.

[b] No basis functions were included on the interstitial site; therefore these values are less certain than the muon hyperfine fields.

TABLE II. Volume derivatives of the muon hyperfine field. Column 1 gives the host and site used in the calculations, o = octahedral, t = tetrahedral interstitial sites. Column 2 gives experimental volume derivatives at 300 K as obtained from hydrostatic pressure experiments (Ref. 26). The site in Fe is unknown. Column 3 gives calculated value. Column 4 gives the contribution from paired states which can be compared with the calculated volume derivative of the nearest-neighbor host moment (column 5) and the experimental value for the pure host (column 6) derived from pressure derivatives (Ref. 27) and compressibility data (Ref. 28).

Host and site	$\frac{d\ln B_{hf}}{d\ln V}$ expt.	$\frac{d\ln B_{hf}}{d\ln V}$ calc.	$\frac{d\ln B_1}{d\ln V}$ calc.	$\frac{d\ln\mu(nn)}{d\ln V}$ calc.	$\frac{d\ln\mu}{d\ln V}$ expt.
bcc Fe o	+0.9	+1.6	+0.8	0.7	0.7
bcc Fe t		+1.2	+1.1	0.8	
fcc Co o	?	−0.6	+0.8	0.4	?
fcc Ni o	+2.7	+0.7	+0.2	1.9	0.4

(iii) The density contributions at the muon (or H) were increased for each unpaired spin orbital.

These results can be understood as follows: The net magnetic moment in Fe, Co, and Ni decreases with pressure because the 3d spin density decreases.[29] This implies a decrease in the exchange polarization forces, and thus a decrease in the magnitude of B_1. The depopulation of states near E_F is expected because of an increase of the mixing matrix elements between the host and impurity states which pushes up some of the antibonding states across E_F. Since the local spin density is positive at E_F (Figs. 2–4), B_2 becomes less positive, opposite to the change in B_1. However, when the local spin density is small at E_F the increase in each orbital density may cancel the depopulation effect and B_2 becomes almost constant or even more positive. This is the case in Fe but the net change is small; the volume dependence mainly arises from the change in B_1. For the octahedral position, we also carried out calculations with the two nearest-neighbor Fe atoms relaxed 5% outwards. A small increase in B_2 was observed while the nearest-neighbor Fe was less perturbed by the impurity charge and its magnetic moment thus increased compared to the unrelaxed case. This gave a more negative B_1. The total hyperfine field was $B_{hf}=-1.30$ T and the volume dependence $d(\ln B_{hf})/d(\ln V)=+0.8$.

In Co the depopulation is the dominant effect, driving B_{hf} more negative when the lattice is compressed. However, it should be pointed out that the volume dependence of the magnetic moment may be underestimated. No experimental value for the cubic phase is known to the authors. In the hexagonal phase the value is $d(\ln B_{hf})/d(\ln V)=1.9$,[27] considerably higher than in Fe and Ni, but there is also a much higher orbital contribution to the magnetic moment[30] than in the cubic structures.

The Ni results are once again very uncertain for the same reasons mentioned earlier, although the sign and order of magnitude are correct.

C. Charge and spin densities

Contour maps of the charge density for several H-impurity clusters are presented in Fig. 5. In Fig. 5(a) a cut through the (110) plane reveals the bond formed between hydrogen and its near neighbors at the octahedral site in bcc iron. This bond is represented primarily by the low-lying state about 9 eV below E_F, as mentioned previously. The H environment is seen to be highly anisotropic. The corresponding interstitial tetrahedral site in Fe is shown in Fig. 5(b), for the (100) plane. The midbond charge density is somewhat lower in this case mainly because of the greater nearest-neighbor distance.

The (110) densities for fcc Co and Ni are shown in Figs. 5(c) and 5(d), respectively. Here the hydrogen–metal bond length is a bit greater, and the resulting bond contains noticeably less charge. Thus, in cobalt the midbond density is $\sim 0.25e/\text{Å}^3$ greater than the interstitial density, while in iron the midbond density is $\sim 0.50e/\text{Å}^3$ greater than the interstitial density.

In order to make more quantitative comparisons, we present radial (spherically averaged) charge and

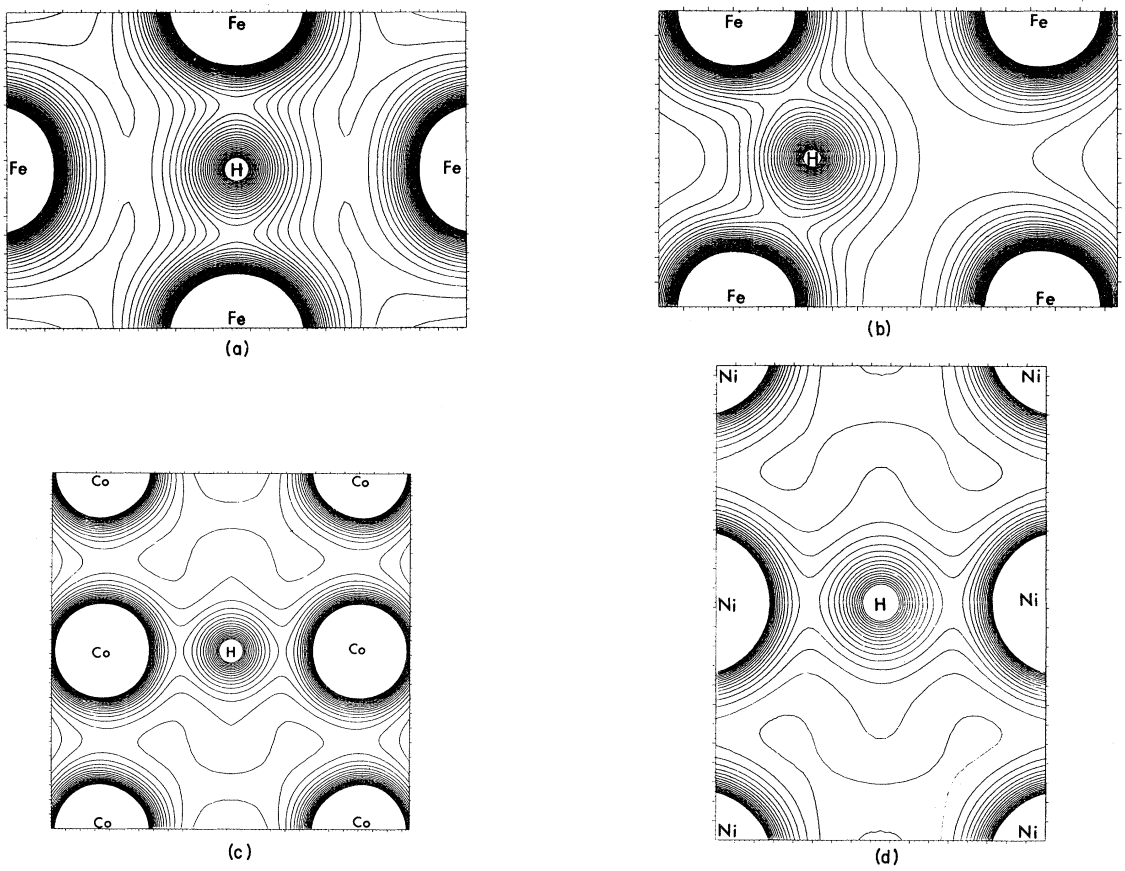

FIG. 5. Charge density maps for (a) (110) plane in Fe through octahedral H site, (b) (100) plane in Fe through tetrahedral H site, (c) (110) plane in Co through octahedral H site, and (d) (110) plane in Ni through octahedral H site. Contour interval is 0.0675 $e/\text{Å}^3$.

spin densities about the hydrogen sites in Fig. 6. In Fig. 6(a) data for the octahedral site in iron are given. In the upper panel appear charge densities ρ for isolated H, the unperturbed Fe_{14} cluster, and the self-consistent solution for HFe_{14}. The pile up of bonding charge at the H site and for some distance away from the proton, exceeds that due simply to superposition. The integrated density (right-hand scale) shows that the proton (or muon) is fully screened at a distance of ~ 1.2 bohr. In the lower panel we see that the spin density of the unperturbed Fe_{14} cluster practically vanishes at the octahedral site, increasing smoothly as one moves out toward the host moment. With the H impurity present, negative polarization is observed, extending out to $R \simeq 0.6$ bohr. Beyond this point the HFe_{14} spin density merges smoothly with that of the unperturbed host. Thus on the scale plotted here, the H-induced spin density damps rather rapidly. Nevertheless, the magnitude of the near-neighbor moment is reduced by $\sim 0.1 \mu_B$.

The results for the Fe tetrahedral site, shown in Fig. 6(b), are superficially quite similar to those for the octahedral site. Here complete charge screening occurs at a slightly larger distance, ~ 1.3 bohr, and the region of negative (minority) spin density persists out to ~ 0.8 bohr. This extended region is partly due to the slight predominance of minority spin in the t site in the iron host.

The corresponding data for octahedral sites in Co and Ni are given in Figs. 5(c) and 5(d). The charge-screening radii are seen to be further increased to ~ 1.4 bohr, and the minority-majority spin crossover moves out to ~ 1.2 and 1.3 bohr, respectively. The charge and spin densities at the H site are seen to be reduced, compared to the iron host, for both Co and Ni. This result is consistent with the relative bond lengths Fe o:Fe t:Co o:Ni o $= 1.43:1.60:1.77:1.73$ Å and host magnetic moments.

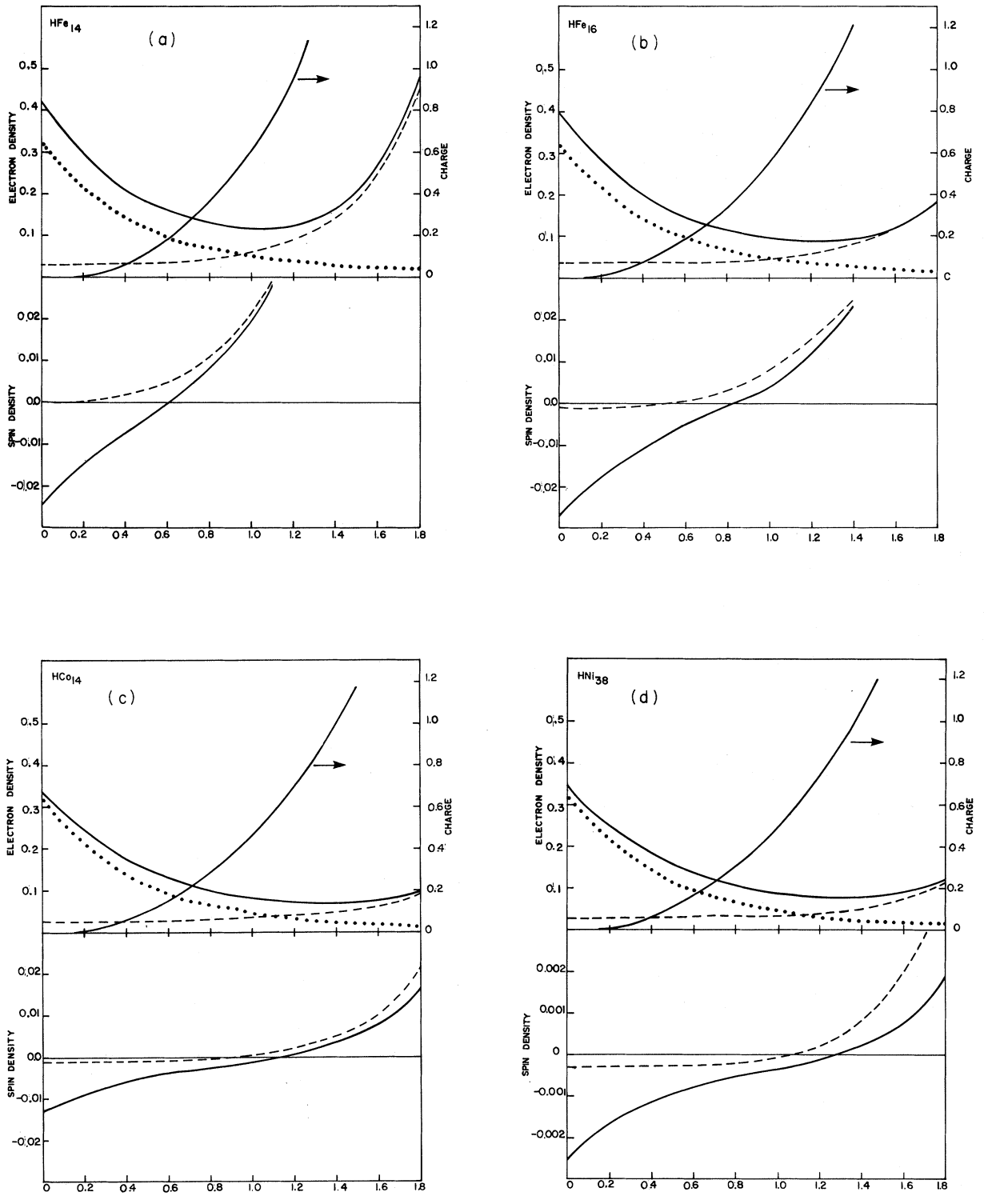

FIG. 6. Radial, spherical averaged charge and spin densities from H site at $\vec{R}=\vec{O}$ for (a) octahedral and (b) tetrahedral sites in Fe and octahedral sites in (c) Co and (d) Ni. Full line shows values obtained with the hydrogen present and dashed lines without the hydrogen. Integrated charge density is shown by the curve associated with the right-hand scale. The dotted curve shows the charge density for a free hydrogen atom.

IV. SUMMARY

The local spin density of interstitial sites in Fe, Co, and Ni was found to critically depend on its energy dependence at the Fermi energy. Molecular-cluster calculations cannot account for this unless a physical model for broadening the discrete energy levels is adopted. The proposed model with an asymptotic condition on the cluster wave functions, gives, in general, a good agreement between calculated and experimental values for the muon hyperfine fields and their pressure derivatives. In particular, the interpretations of the underlying mechanisms are easy to make with the LCAO-type of basis wave functions and a separation into paired and unpaired contributions.

Lattice relaxation around the impurity was not found to be important and the effect can be estimated from the volume dependence of the hyperfine field as measured through pressure experiments.

The large zero-point motion of the muon was not accounted for and the finite extent of the muon wave function can have a substantial effect on the hyperfine field.[31] As the muon samples regions closer to host atoms, effects similar to those discussed in connection with the uniformly compressed lattice will appear: i.e., destabilization of near-neighbor host moment and depopulation of antibonding states near E_F. These effects work in opposite directions, so real quantitative estimates are not possible. However, we speculate that zero-point motion leads to a shift in the hyperfine field similar to that of a contracted lattice.

ACKNOWLEDGMENTS

The work of one of the authors (B.L.) was supported by a Swedish National Research Council Fellowship and by the National Science Foundation (Grant No. DMR79-25379). Use of the facilities of the Materials Research Center is gratefully acknowledged.

APPENDIX

The Green's-function formalism provides a physically understandable alternative derivation of Eq. (13), giving expansion coefficients in terms of the asymptotic wave function. We begin with the usual zeroth-order Hamiltonian and eigenfunctions satisfying

$$(H^0-E)\psi_E^0=0 \tag{A1}$$

with the related Green's-function equation

$$(H^0-E)G_E(\vec{r},\vec{r}')=-\delta(\vec{r}-\vec{r}') \ . \tag{A2}$$

Identifying the function ψ_E^0 with ϕ_k [see Eq. (12)] we then introduce the perturbation $u(\vec{r})=V_{\text{cluster}}-V_0$ and write down the solution of the Schrodinger equation for the cluster potential as

$$\psi_{E,k}=\phi_k+\int G_E(\vec{r},\vec{r}')u(r')\psi_{E,k}(r')d^3r' \ . \tag{A3}$$

Taking the trial wave function

$$\psi_{E,k}=\phi_k+\sum_i c_i\Phi_i$$

and operating on (A3) with (H^0-E), gives

$$\sum_i c_i(H^0-E)\Phi_i=u(\vec{r})\left[\phi_k(\vec{r})+\sum_i c_i\Phi_i(\vec{r})\right] .$$

Rearranging, one obtains

$$\sum_i c_i(H-E)\Phi_i=-u(\vec{r})\phi_k(\vec{r}) \ , \tag{A4}$$

where H is the cluster Hamiltonian. Taking the inner product with every function Φ_j, and introducing the amplitude a_k, we obtain Eq. (13).

In this picture the propagating state ϕ_k is perturbed by its interaction with the cluster potential. This perturbation causes a mixing with cluster states Φ_i, which becomes large for $E\approx E_i$. By separating the result into orthogonal cluster-localized and long-range components, we are able to give an account of the energy broadening of the cluster levels needed for interpretation of local properties.

---

* Present address: Department of Physics, Uppsala University, Box 530, S-75121 Uppsala, Sweden.

[1]For a review see, e.g., P. F. Meier, Hyperfine Interact. 8, 591 (1981); W. Kündig, *ibid.* 9, 571 (1981); E. Karlsson, Nucl. Sci. Appl. 1, 57 (1980).

[2]For a review see, e.g., R. M. Nieminen, Hyperfine Interact. 8, 437 (1981).

[3]W. A. Harrison, *Pseudopotential in Theory of Metals* (Benjamin, New York, 1966).

[4]J. Friedel, Philos. Mag. 43, 153 (1952); A. Sjölander and M. J. Stott, Phys. Rev. B 5, 2109 (1972); P. Bhattacharya and K. S. Singwi, Phys. Rev. Lett. 29, 22 (1972); A. K. Gupta, P. Jena, and K. S. Singwi, Phys. Rev. B 18, 2712 (1978).

[5]Z. D. Popović, M. J. Stott, J. P. Carbotte, and G. R. Pierecy, Phys. Rev. B 13, 590 (1976); C. O. Almbladh, U. von Barth, Z. D. Povović, and M. J. Stott, *ibid.* 2250 (1976); E. Zaremba, L. M. Sander, H. B. Shore, and J. H. Rose, J. Phys. F 7, 1763 (1977).

[6]P. Jena and K. S. Singwi, Phys. Rev. B 17, 3518 (1978).

[7]P. Jena and M. Manninen, Hyperfine Interact. 9, 405 (1981); M. Manninen and R. M. Nieminen, J. Phys. F 9, 1333 (1979).

[8]See, e.g., J. L. Beeby, Proc. R. Soc. London 302, 113 (1967); P. Soven, Phys. Rev. 151, 539 (1966); R. Zeller and P. Dederichs, Phys. Rev. Lett. 42, 1813 (1979).

[9]J. Keller, J. Phys. C 4, 3143 (1971); in *Proceedings of the Third International Conference on Computers in Chemical Research, Education, and Technology, Venezuela, 1976,* edited by E. V. Ludeera, N. Sabelli, and A. C. Wahl (Plenum, New York, 1977), p. 225.

[10]N. Rösch in, *Electrons in Finite and Infinite Structures,* edited by P. Phariseau (Plenum, New York, 1977).

[11]V. I. Anisimov, V. A. Gubanov, D. E. Ellis, and E. Z. Kuramaev, J. Phys. F 11, 405 (1981).

[12]J. Keller, Hyperfine Interact. 6, 15 (1979); B. D. Patterson and J. Keller, *ibid.* 6, 73 (1979).

[13]J. Kanamori, H. K. Yoshida, and K. Terakura, Hyperfine Interact. 8, 573 (1981).

[14]O. Jepsen, R. M. Nieminen, and J. Madsen, Solid State Commun. 34, 575 (1980).

[15]E. J. Baerends, D. E. Ellis, and P. Ros. Chem. Phys. 2, 41 (1973); F. W. Averill and D. E. Ellis, J. Chem. Phys. 59, 6412 (1973); A. Rosén and D. E. Ellis, *ibid.* 65, 3629 (1976).

[16]D. E. Ellis and G. S. Painter, Phys. Rev. B 2, 2887 (1970).

[17]U. von Barth and L. Hedin, J. Phys C 5, 1629 (1972).

[18]V. L. Moruzzi, J. F. Janak, and A. R. Williams, *Calculated Electronic Properties of Metals* (Pergamon, New York, 1978).

[19]B. Delley and D. E. Ellis, J. Chem. Phys. 76, 1949 (1982).

[20]E. O. Wollan, J. W. Cable, and W. C. Koehler, J. Phys. Chem. Solids 24, 1141 (1963).

[21]A. Möslang, H. Graf, E. Recknagel, A. Weidinger, Th. Wichert, and R. I. Grynszpan, in Proceedings of the Yamada Conference V, Kyoto, 1981 (in press), and private communication.

[22]Following Schönflies notation, see, e.g., M. Tinkham, *Group Theory and Quantum Mechanics* (McGraw-Hill, New York, 1964).

[23]R. S. Mulliken, J. Chem. Phys. 23, 1833 (1955); 23, 1841 (1955).

[24]C. G. Shull and Y. Yamada, J. Phys. Soc. Jpn. 17, Suppl. B-3,1 (1962); C. G. Shull and H. A. Mook, Phys. Rev. Lett. 16, 184 (1965); R. M. Moon, Phys. Rev. 136, A195 (1964); H. A. Mook, *ibid.* 148, 495 (1966).

[25]See, e.g., discussion following paper by G. Balzer, H. Graf, T. Möslang, E. Recknagel, A. Weidinger, and R. E. Grynszpan, Hyperfine Interact. 9, 589 (1981).

[26]T. Butz, J. Chappert, J. F. Dufresne, O. Hartmann, E. Karlsson, B. Lindgren, L.O. Norlin, P. Podini, and A. Yaouanc, Phys. Lett. 75A, 321 (1980).

[27]D. Bloch and R. Pauthenet, J. Appl. Phys. 36, 1229 (1965).

[28]K. Gschneidner, Jr., Solid State Phys. 16, 275 (1964).

[29]J. F. Janak, Phys. Rev. B 20, 2206 (1979).

[30]D. S. Rodbell, J. Phys. Soc. Jpn. 17, Suppl. B-1, 313 (1962).

[31]S. Estreicher, A. B. Denison, and P. F. Meier, Hyperfine Interact. 8, 601 (1981).